Interfaces: Adsorption, Reactions, Films, Forces, Measurement Techniques, Charge Transfer, Electrochemistry, Electrocatalysis, Energy Production and Storage

Flexible ultraviolet and ambient light sensor based on nanomaterial network fabricated by using selective and localized wet-chemical reactions

Daejong Yang, Jaehwan Lee, Donghwan Kim, Incheol Cho, Jong G. Ok, and Inkyu Park

Langmuir, **Just Accepted Manuscript** • DOI: 10.1021/acs.langmuir.7b02332 • Publication Date (Web): 14 Mar 2018

Flexible ultraviolet and ambient light sensor based on nanomaterial network fabricated by using selective and localized wet-chemical reactions

Daejong Yang[1,2,3], Jaehwan Lee[1,2], Donghwan Kim[1,2], Incheol Cho[1,2], Jong G. Ok[4], and Inkyu Park[1,2,]*

[1] Department of Mechanical Engineering, Korea Advanced Institute of Science and Technology (KAIST), Daejeon 34141, South Korea

[2] KI for the NanoCentury, Korea Advanced Institute of Science and Technology (KAIST), Daejeon 34141, South Korea

[3] Department of Medical Engineering, California Institute of Technology, Pasadena, CA 91125, United States

[4] Department of Mechanical and Automotive Engineering, Seoul National University of Science and Technology, Seoul 01811, South Korea

ABSTRACT

We report ZnO nanowire and TiO_2 nanotube based light sensors on flexible polymer substrates fabricated by localized hydrothermal synthesis and liquid phase deposition (LPD). This method realized simple and cost-effective in-situ synthesis and integration of one-dimensional ZnO and TiO_2 nanomaterials. The fabricated sensor devices with ZnO nanowires and TiO_2 nanotubes show very high sensitivity and quick response to the ultraviolet (UV) and ambient light, respectively. In addition, our direct synthesis and integration method result in mechanical robustness under external loading such as static and cyclic bending because of the strong bonding between nanomaterial and electrode. By controlling the reaction time of LPD process, Ti:Zn ratio could be simply modulated, and the spectral sensitivity to the light in the UV to visible range could be controlled.

KEYWORDS

nanomaterial integration, UV sensor, light sensor, flexible sensor, nanowire, zinc oxide, titanium oxide

INTRODUCTION

One-dimensional (1D) nanomaterials such as nanowires and nanotubes have attracted a great deal of attention due to their novel properties and versatile applications such as field effect transistor,[1] energy generation,[2,3] energy storage,[4] field emission[5] and physical/chemical sensing.[6-8] Especially, they have shown great potentials for sensing applications due to their unique physical and chemical properties such as high crystallinity,[9,10] versatile chemical compositions,[11] tunable bandgap,[12,13] chemical reactivity,[14] small dimension, and high surface to volume ratio.[15,16] Due to these advantages, many 1D nanomaterial sensors have been widely developed.[17-19] In particular, ZnO is an n-type semiconductor material with a wide direct bandgap energy of 3.37 eV and large exciton binding energy of 60 meV, which makes it an outstanding material for photonic sensing in the UV range.[20] S. Bai, et al.[21] fabricated ZnO nanowire based UV photodetectors with ultra-high sensitivity ($I/I_0 > 10^5$). In addition, M.R. Alenez, et al.[22] made ultra-fast ($\tau < 100$ ms) ZnO nanowire based UV photodetectors.

Especially in the electrical device applications, 1D nanomaterials have to be assembled and integrated on device electrodes in the electrical circuit. The most common method to connect 1D nanomaterials and electrodes is drop casting of nanomaterial solution onto the electrodes.[23] Although this is a very simple and cost-effective integration method, it only produces randomly dispersed nanowire networks and provides limited patterning resolution (minimum diameter ~ 1 mm) and thus is not suitable for highly integrated, ultra-compact devices.[24,25] For more accurate and delicate device integration of 1D nanomaterials, numerous methods such as screen printing,[26,27] inkjet printing,[28] contact printing,[21,29] optical trapping,[30] atomic force microscope (AFM)[31], electrostatic force,[32] magnetic force[33] and dielectrophoresis[34] have been utilized. The printing methods such as screen printing and inkjet printing are simple but provide limited resolutions (minimum diameter ~ 100 μm). Optical trapping and AFM based methods provide much higher integration accuracy but

require expensive equipment and allow limited throughput. Since the methods based on magnetic, electrostatic or dielectrophoretic force use liquid suspension of nanomaterials, deposition of nanomaterials can occur at undesired locations via nonselective physical adsorption. Moreover, abovementioned methods provide only the alignment and placement of nanomaterials, not the reliable bonding between nanomaterials and electrodes, and therefore mechanical robustness cannot be guaranteed.

In order to solve these technical issues of controlled and reliable integration of 1D nanomaterials for the fabrication of highly integrated sensors, we have developed a novel and facile method for the in-situ synthesis and integration in selected locations using sequential localized liquid-phase reactions.[18,35] The fabrication processes have been specially designed for flexible substrates to widen the application of this method. In addition, numerical analysis on flexible substrates has also been discussed in detail. As shown in Figure 1, the microheater generates a local hot spot by Joule heating and nanowires are synthesized on the surface of the microheater. The local heating induces convective flow of precursor solution and enables continuous and localized synthesis of the nanowires. In this work, we applied this method to the synthesis of ZnO nanowires. After the synthesis of ZnO nanowires, they were converted to TiO_2 nanotubes by room temperature liquid phase reaction within TiO_2 precursor solution. Since these reactions occur at very low temperature (< 100 °C), and use mild and non-corrosive chemicals, nanomaterials can also be directly synthesized on flexible polymer substrates. The most significant advantages of this method are (1) direct synthesis and integration of nanomaterials without further assembly and integration processes required, (2) simple and low-cost setup for process, (3) operation in low temperature, liquid and atmospheric pressure condition, and (4) mechanically and electrically robust bonding between synthesized nanomaterials and electrodes. All of these advantages can play as essential factors for the application to flexible electronic devices.

MATERIALS AND METHODS

Fabrication of microheater platform: 75 μm thick polyimide (PI, PIF075, Shinmax Technology Ltd., Taiwan) was used as the substrate for the fabrication of flexible light sensor. The microheaters were fabricated using conventional photolithography and metal lift-off processes. Photoresist (AZ9260, MicroChemicals GmbH, Germany) was first coated on the silicon (Si) wafer and polyimide (PI) film was attached on the Si wafer using the spin-coated photoresist as a temporary adhesive. Photoresist (AZ5214, MicroChemicals GmbH, Germany) was patterned for microheaters and pads on the PI film using photolithography process. 10 nm thick chrome (Cr) was deposited as the adhesion layer and 200 nm thick gold (Au) film was also deposited on the substrate by electron beam evaporation. The substrate was immersed in the acetone to remove the photoresist pattern and dummy Cr/Au film. Finally, PI film was separated from the Si wafer.

Synthesis of ZnO nanowires: Two methanol based solutions consisting of 10 mM zinc acetate dihydrate ($Zn(CH_3COO)_2{\cdot}2H_2O$) and 30 mM potassium hydroxide (KOH) were prepared and heated to 60 ºC. The volumetric ratio of the former and the latter was 25:13. The KOH solution was added dropwise to the zinc acetate dihydrate solution while maintaining temperature. The mixture was stirred for 2 hours at 60 ºC.[36] The microheater platforms were coated with ZnO nanoparticle solution and heated to 150 °C on a hotplate for 20 minutes. 25 mM zinc nitrate hydrate ($Zn(NO_3)_2{\cdot}6H_2O$), 25 mM hexamethylenetetramine (HMTA, $C_6H_{12}N_4$) and 6 mM polyethylenimine (PEI, $(C_2H_5N)_n$) were mixed in the deionized (DI) water as the precursor solution for the ZnO nanowire synthesis. (All chemicals were purchased from Sigma-Aldrich.) A small PDMS well was attached on the microheater device and filled with 10 μL of the ZnO nanowire precursor solution. A DC bias of 0.28 V was

applied to the microheaters for 30 minutes for a Joule heating. All the synthesis process was monitored in real-time by high resolution optical microscope (BX51M, Olympus, Japan).

Synthesis of TiO_2 nanotubes: The precursor solution consisting of 0.3 M boric acid (H_3BO_3) and 0.1 M ammonium hexafluorotitanate ($(NH_4)_2TiF_6$) in DI water was prepared for the synthesis of TiO_2 nanotubes (All chemicals were purchased from Sigma-Aldrich.). A PDMS well was attached on the microheater device with pre-synthesized ZnO nanowires and 10 μL of TiO_2 precursor solution was supplied for 15 minutes at room temperature with no additional heating.

Optical characterization of ZnO-TiO_2 nanocomposite: ZnO nanowires were synthesized on a cover glass (Cover Slips (22 mm × 22 mm), Duran Group, Germany) to measure the absorption spectra. Single sides of six sheets of the cover glass were coated with ZnO nanoparticle solution and heated at 150 °C on a hotplate for 20 minutes to form a ZnO seed layer. They were immersed in the ZnO precursor solution and heated at 95 °C for 10 hours while refreshing the precursor solution every 2.5 hour in a convection oven. After the synthesis of ZnO nanowires, five samples were dipped into the TiO_2 precursor solutions for 10, 20, 40, 60 and 120 minutes to obtain ZnO-TiO_2 composites with various Zn:Ti ratios. UV-VIS-NIR spectrophotometer (V-570, Jasco Inc., USA) was utilized to measure the absorption spectra of seven samples (reference cover glass, ZnO nanowire and five ZnO-TiO_2 composites on the cover glass substrates). The absorption spectra of cover glass were subtracted to remove the substrate effect.

Measurement of sensor response to ultraviolet (UV) and ambient light sources: The electrical characterization of devices was carried out using a potentiostat/galvanostat (CHI600D, CH Instruments Inc., USA). A UV lamp with a peak wavelength of λ=365 nm (LF206LS, UVitec Cambridge, United Kingdom) and an ambient light LED with the color rendering index of 94 and color temperature of 5500 K (NL200, HAREX, South Korea) were

employed as UV and ambient light sources. DC bias of 0.5 V and 5 V were applied to ZnO nanowire and TiO_2 nanotube devices, respectively, and the currents through the nanomaterials were measured under various light intensities.

Bending test: The bending test of the ZnO nanowire and TiO_2 nanotube device on a flexible PI substrate were conducted using a custom-made bending system consisting of a linear stage and a carrier film (polyester film with 0.5 mm thickness). The light sensors were attached on the carrier film, whose ends were connected to the linear stage. The film was bent with various radii of curvature by moving the linear stage.

RESULTS AND DISCUSSIONS

The fabrication of ZnO nanowire based UV sensor relies on the localized hydrothermal reaction. The microheaters designed to generate highly localized heating were fabricated using photolithography and metal deposition processes. As shown in Figure S1a, a pair of microheaters with a length of 30 μm, a width of 3 μm, a thickness of 200 nm, and a gap of 4 μm was located at the center of device. The most important factor for local hydrothermal synthesis is the temperature localization. The numerical simulation result indicates that the thermal power density (power per unit area) is 308,000 times larger in the microheater than in the contact pads during Joule heating due to the large electrical resistance of the microheater (see Figure S1b in the Supplementary Information). This concentrated heat generation enables localized endothermal chemical reaction in the liquid precursor environment.

Figure panels 2a-b show the schematic of synthesis process for ZnO nanowires by using localized hydrothermal reaction. The synthesis mechanism is the same as that for general hydrothermal synthesis of ZnO nanowires, except for the localized reaction driven by Joule heating.[35] The solubility of ZnO in the precursor decreases at higher temperature and therefore ZnO nanowires are synthesized by endothermic chemical reaction.[37] The ZnO

nanowire bundles grown from two neighboring microheaters become longer and eventually form an interconnection with each other. Figure panels 2c-e and S3a,b show the photo and SEM images of locally synthesized ZnO nanowires on PI substrate. The ZnO nanowires can be synthesized on the flexible polymer substrate due to the low seeding (150 °C) and synthesis temperature (~95 °C), and non-harsh chemicals used for the liquid-phase reaction. Crystalline ZnO nanoparticles with an average diameter of 3 nm were used as seeds[36] and the seed layer did not show any electrical current due to the electrical disconnection between the particles (see Figure S4 in the Supplementary Information). The average diameter and length of ZnO nanowires were 200 nm and 4 μm, respectively. As shown in the cross-sectional SEM images of the ZnO in Figure S2a,b, ZnO nanowires were directly synthesized on the surface of gold electrode, which enabled a close connection between nanowires and electrode. Two ZnO nanowire bundles were connected with each other at the center of two microheaters in the form of a bridge, which can be used as the electrical path for the UV sensor.

The synthesis processes were analyzed by finite element method (FEM) simulation of Joule heating and convective heat / mass transfers. The numerical simulation was conducted by COMSOL Multiphysics® with "electric current" and "non-isothermal flow" modules. As shown in Figure S3a, DC bias was applied to the microheater and heat generation was calculated by "electric current" module. The calculated heat was applied to the heat source in the "non-isothermal flow" module, from which temperature profile and flow of precursor solution were calculated. A local hot spot (maximum temperature=95.1 °C) was generated at the microheaters and this non-uniform temperature caused a convective flow of precursor solution (Figure 2f,g). In order to verify the thermal insulation effect of the PI substrate, we conducted the same numerical simulation with a silicon (Si) substrate with sufficiently thick (5 μm) insulation layer. Figures S3b,c show the temperature profile and flow motion of the

precursor solution on the SiO_2/Si substrate. Even though the same electrical bias was applied and the same amount of heat was generated, the temperature at the microheater only rose by 27.1 °C from the initial temperature (20 °C). This is because the thermal conductivity of PI (0.18 W/(m·K) at 300 K)[38] is 800 times lower than that of Si (142.2 W/(m·K)[39] and 6 times lower than that of SiO_2 (1.063 W/(m·K)[40] at 300 K). As a result, PI could effectively isolate thermal energy and thus generated higher local temperature even by consuming lower energy. Therefore, the usage of polymer substrate not only widens the flexible device applications, but also helps the reduction of energy consumption during synthesis and possible side effects (eg. electrodeposition[41] and electrolysis[42]) originating from the high electrical bias applied in the liquid environment.

The current-voltage (I-V) curve of ZnO nanowires verified that nanowires were successfully synthesized on the electrodes and formed an electrical interconnection between electrodes (Figure 2h). Because the work function of ZnO (4.5 eV)[43] is lower than that of gold electrode,[44] the I-V curve shows a Schottky contact behavior.[45-47] The bandgap energy of ZnO is 3.37 eV that corresponds to a wavelength of 365 nm.[21] Thus, ZnO can show responses to different intensities of UV light by photoconductive effect, which is related to the electron-hole pair generation and chemisorption/desorption of oxygen on the surface of the sensing materials.[48] In the dark state, oxygen molecules are chemisorbed on the ZnO surface as O_2^- ions by capturing free electrons from the ZnO, and this generates a depletion layer near the surface.[49,50] When semiconductor materials absorb photon energy above their bandgap, pairs of electrons and holes are generated. The holes generated by photons combine with chemisorbed oxygen ions existing on the surface of ZnO. The oxygen ions are converted to oxygen molecules (O_2) and then migrate from the surface of ZnO. In this process, free electrons are returned back to ZnO and play as mobile charge carriers. Furthermore, the electrons generated by photons also contribute to the electrical current as mobile charge

carriers. Consequently, the concentration of mobile charge carriers is increased and the width of depletion layer is decreased.[49] Due to this surface reaction mechanism and high surface to volume ratio, one-dimensional nanomaterials such as nanowires and nanotubes provide much higher sensitivity and response speed than the bulk materials.[51,52] Figure 2i shows the real-time response of ZnO nanowire sensor to the UV light with various intensities. The dark current of 19.1 nA was amplified to 2.54 μA under the light intensity of 1.29 mW/cm^2 with 19.4 sec of the rise time ($\tau_{r,90\%}$) and 16.7 sec of decay time ($\tau_{d,10\%}$). The current through the ZnO nanowire interconnection exhibited an incremental change by stepwise change of UV light intensities. As shown in Figure 2j, the relationship between photocurrent and UV intensity obeys a power law,[48,53] $I=\alpha \cdot J^n$, where I is the photocurrent [μA], J is the intensity of UV light [mW/cm^2], and α (6.2101×10^{-7}) and n (0.5563) are coefficients.

In order to use the flexible sensors in practical applications, the devices must be robust under mechanical stresses. The mechanical robustness and UV light sensing characteristics of the flexible ZnO nanowire sensor device was tested in bending conditions. The device was initially in a flat condition but bent to various curvature radii (ρ = 46.0 and 6.8 mm) while UV lamp was turned off and on with an intensity of 0.39 mW/cm^2. As shown in Figure 3a, the average on/off ratios (I_{on}/I_{off}) are 113.1, 107.5, 100.7, 107.6 and 116.0 in a flat condition, in bent conditions with curvature radii of 46.0 mm, 6.8 mm and 46.0 mm, and back in a flat condition, respectively. Figure 3b shows the response after 100 and 1,000 cycles of bending with a curvature radius of 6.8 mm. The average on/off ratio before bending and after 100 and 1,000 cycles of bending were 122.6, 115.5 and 115.7, respectively. The sensing performance was maintained with little degradation by bending condition with various radii of curvature and repeated bending cycles. Figure 3c and S5 shows the shapes of ZnO nanowire network in a flat condition and under various curvature radii of 71.9, 46.0, 26.1, 16.6, and 6.8 mm. In these images, no destruction or damages can be found in the nanowire network by bending.

In addition, the ZnO nanowire junction withstand with no observable changes after 1,000 cycles of repeated bending with a curvature radius of 6.8 mm. We also have conducted bending test along the transverse direction to the microheaters. Similar to the bending in longitudinal direction, the electrical current fluctuated within 10 % during the sequential bending down to a curvature radius of 6.8 mm (see Figure S6 in the Supplementary Information).

These results indicate strong mechanical stability of ZnO nanowire junctions and robust bonding between synthesized ZnO nanowires and metal electrode. These excellent mechanical characteristics can be attributed to the direct synthesis on substrate and vertically grown structures of nanowire array. The nanowires were directly synthesized from the nucleation points on the surface of electrode by forming crystallized structures, thereby providing stronger bonding to the electrode than the Van der Waals or electrostatic forces that exist between the electrodes and ex-situ grown, subsequently assembled nanostructures (i.e. nanostructures assembled on the electrodes by conventional integration methods such as drop casting, dielectrophoresis or micro-contact printing). As mentioned above, another reason for the mechanical robustness of ZnO nanowires is the vertically grown structure with respect to the substrate. Since we have fabricated small-sized sensor, the amount of absolute deformation is very small. However, the strain is the same regardless of the size of structure under the same curvature radius. Under bending condition, three dimensional bridging structures fabricated in this work are effective in reducing stress. As shown in Figure S7a,b, the bending stress in nanowires is proportional to the angle of bending and inversely proportional to the length of nanowire if pure bending condition is assumed. Under the same bending condition, vertically grown nanowires provides larger root-to-junction length and thus reduces bending stresses as compared to horizontally grown nanowires (see Section 4 in the Supplementary Information).[54]

Not only ZnO nanowires but also TiO_2 nanotubes can be used as light sensors due to their wide bandgap (anatase 3.2 eV, rutile 3.0 eV).[55] The synthesis method of TiO_2 nanotubes is also based on the localized wet chemical reactions.[55] This method consists of two steps: localized hydrothermal reaction for the synthesis of ZnO nanowires and liquid phase deposition (LPD) process of TiO_2 nanotubes using ZnO nanowires as templates. As shown in Figure 1, pre-synthesized ZnO nanowires are used as templates for the reaction in TiO_2 precursor solution. The synthesis mechanism of TiO_2 nanotubes via LPD method consists of two parallel reactions: TiO_2 deposition and ZnO etching. TiO_2 is deposited on the surface of ZnO nanowires by hydrolysis reaction of titanium-fluoro complex ion (TiF_6^{2-}) from ammonium hexafluorotitanate (AHFT). This reaction generates fluoride (F^-) ions that are combined with boric acid and accelerates the hydrolysis reactions.[56,57] The ZnO nanowires are coated with the TiO_2 nanofilm and the TiO_2/ZnO core-sheath nanostructures are acquired. Simultaneously, the ZnO nanowire templates are etched by the acidic precursor solution.[58] Figure panels 4a-f show the SEM images and EDS data of pre-synthesized ZnO nanowires and TiO_2 nanotubes converted from the ZnO nanowire template. It can be observed that the shape of ZnO nanowire templates are maintained in the TiO_2 nanotube bundle. However, the outer diameter of the TiO_2 nanotubes are several tens of nanometers thicker than the ZnO nanowires due to the thickness of deposited TiO_2 nanotube film. Figure panels S2c,d show the cross-sectional SEM image of TiO_2 nanotube device. The slightly rough structures were made during the conversion process, which indicates that the TiO_2 precursor reached to the root of ZnO nanowires bundle and ZnO nanowires were converted to TiO_2 nanotube. The image shows a close connection between TiO_2 nanotube and Au electrode. As shown in the TEM image of TiO_2 nanotube (Figure 4g) and EDS data (Figure 4f), TiO_2 nanotubes show obvious tubular nanostructure with a Ti:Zn ratio of 0.923:0.077. These results indicate that the ZnO nanowires were mostly removed during the conversion process, but small amount of

Zn still remained after the reaction. The HRTEM image shows that the material is a mixture of mostly polycrystalline and partially amorphous crystalline structures (Figure 4h). The lattice spacing of crystallized region is 3.54 Å that corresponds to the (101) plane of the typical anatase TiO_2.[59]

TiO_2 materials are typically used for UV light sensors due to their bandgap corresponding to the wavelength of UV light (eg. bandgap of anatase TiO_2=3.2 eV).[54] However, their photoelectric properties can be tuned by introducing Zn impurities to realize ambient light sensors.[60-62] In our process, small amount of Zn remained after the synthesis of TiO_2 nanotubes as explained above, thereby Zn impurity within TiO_2 nanotubes is realized without further doping process required. In order to analyze the photonic characteristics of ZnO and ZnO-TiO_2 composites, their absorption spectra were measured. As shown in Figure 5a, six samples with different atomic ratios of Ti:Zn from 0:100 to 97:3 were prepared by increasing the conversion time on the glass substrate. Figure panels 5b,c show the absorption spectra and absorbance ratio of visible (380-820 nm) to UV (< 380 nm) light region for the ZnO nanowire and TiO_2 nanotube samples. The absorbance in the UV region did not show significant change, whereas that in the visible region was gradually increased by 13 %, 16 %, 28 %, 58 % and 63 % for the samples with atomic concentration of Ti in 18.1 %, 66.4 %, 83.9 %, 89.4 % and 96.6 %, respectively, than the pristine ZnO nanowires. Therefore, the absorbance ratio of visible to UV region ($I_{visible}/I_{UV}$) was increased with increasing Ti to Zn ratio. Zn atoms and oxygen vacancies could not be perfectly removed inside the TiO_2 nanotubes by the LPD method. However, these impurities can be helpful to increase the absorption of visible light in the TiO_2 nanotubes. The oxygen vacancy states are located between the valence and conduction bands of TiO_2, locating at 2.02-2.45 eV above the valence band, which corresponds to a wavelength of 506-614 nm.[60,61] In addition, the Zn related defects in the TiO_2 nanotubes contribute to the absorption in the wavelength of 410-

490 nm.[61] In summary, Zn defects generate intermediate bandgap levels between valance and conduction bands and thus reduce required energies to excite electrons to the conduction band (Figure 5d).

In order to verify the mechanical robustness of the TiO_2 nanotube device, it was bent to a curvature radius of 6.8 mm and recovered to a flat condition while measuring the electrical current. As shown in Figure 6a, the current was stable during static bending with different curvature radii. Figure 6b shows the current through TiO_2 nanotube device after bending cycles of 10, 100 and 1,000 times. There were only 2 % current drop after 1,000 times of repeated bending, which indicates no damage or deformation in the TiO_2 nanotube device during repeated bending.

The resistance of the TiO_2 nanotube sensor was measured under various illuminance of ambient light. The sensing mechanism of the TiO_2 nanotube sensors is similar to that of the ZnO nanowire sensors. By the exposure to the ambient light, the electron-hole pairs are generated and surface adsorbed oxygen ions are converted into O_2 molecules and then desorbed from the surface of TiO_2 nanotubes.[63,64] The I-V curve shown in Figure 6c indicates very weak Schottky contact between TiO_2 nanotube bundles and electrodes under dark state. Generally, contact between TiO_2 and gold shows Schottky behavior because work function of TiO_2[65] is lower than that of gold.[43] However, in this work, the Zn impurities and oxygen vacancies filled the bandgap of TiO_2 and Fermi level was adjusted as a consequence. Figure 6d shows the real-time response of TiO_2 nanotube sensor to the ambient light. The dark current of 62.9 pA was amplified by 8.92 and 10.82 times under 4,300 and 16,900 lx of ambient light. The current through TiO_2 nanotubes were increased by higher illuminance of ambient light (Figure 6e). As shown in Figure 6f, the TiO_2 nanotube exhibit rapid response to turn-on and turn-off cycles under 16900 lx ambient light. The rise time ($\tau_{r,90\%}$) and decay time ($\tau_{d,10\%}$) are 0.16 s and 0.35 s, respectively. The hollow structures of TiO_2 nanotubes

shorten the electron path to the surface of nanostructures, which reduces the recombination probability.[66,67] Large number of electrons can quickly reach the oxygen molecules, and this reduces the rise time and decay time.

CONCLUSIONS

We have developed ZnO nanowire based UV light sensor and TiO_2 nanotube based ambient light sensor on flexible substrates by using localized hydrothermal synthesis of ZnO nanowires and liquid phase deposition process of TiO_2 thin films on the ZnO nanowire templates. The ZnO nanowire and TiO_2 nanotube sensors exhibited sensitive and rapid sensing response to UV and ambient light, respectively. Moreover, the devices showed reliable light sensing performance under mechanical stress due to the robust connection between nanowires and electrodes resulting from the direct synthesis process. They would be very useful for the sensors in wearable and internet of things (IoT) applications due to their simple and low-cost fabrication methods, ultra-compact form factors, mechanical robustness, and ultra-low power consumption.

FIGURES

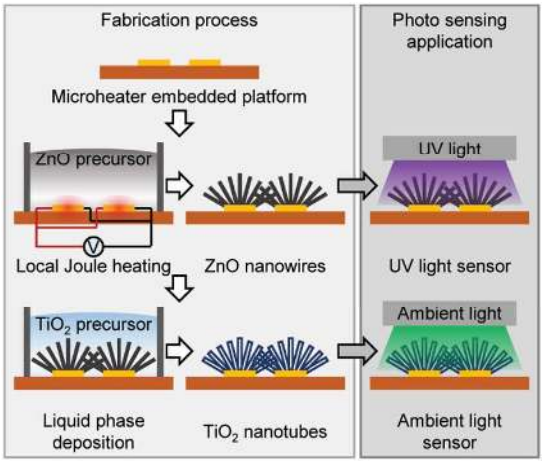

Figure 1. Schematic of process flow for the ZnO nanowire and TiO_2 nanotube synthesis. ZnO nanowires are synthesized by local hydrothermal reaction along microheaters and pre-synthesized ZnO nanowires are converted to TiO_2 nanotubes by liquid phase deposition.

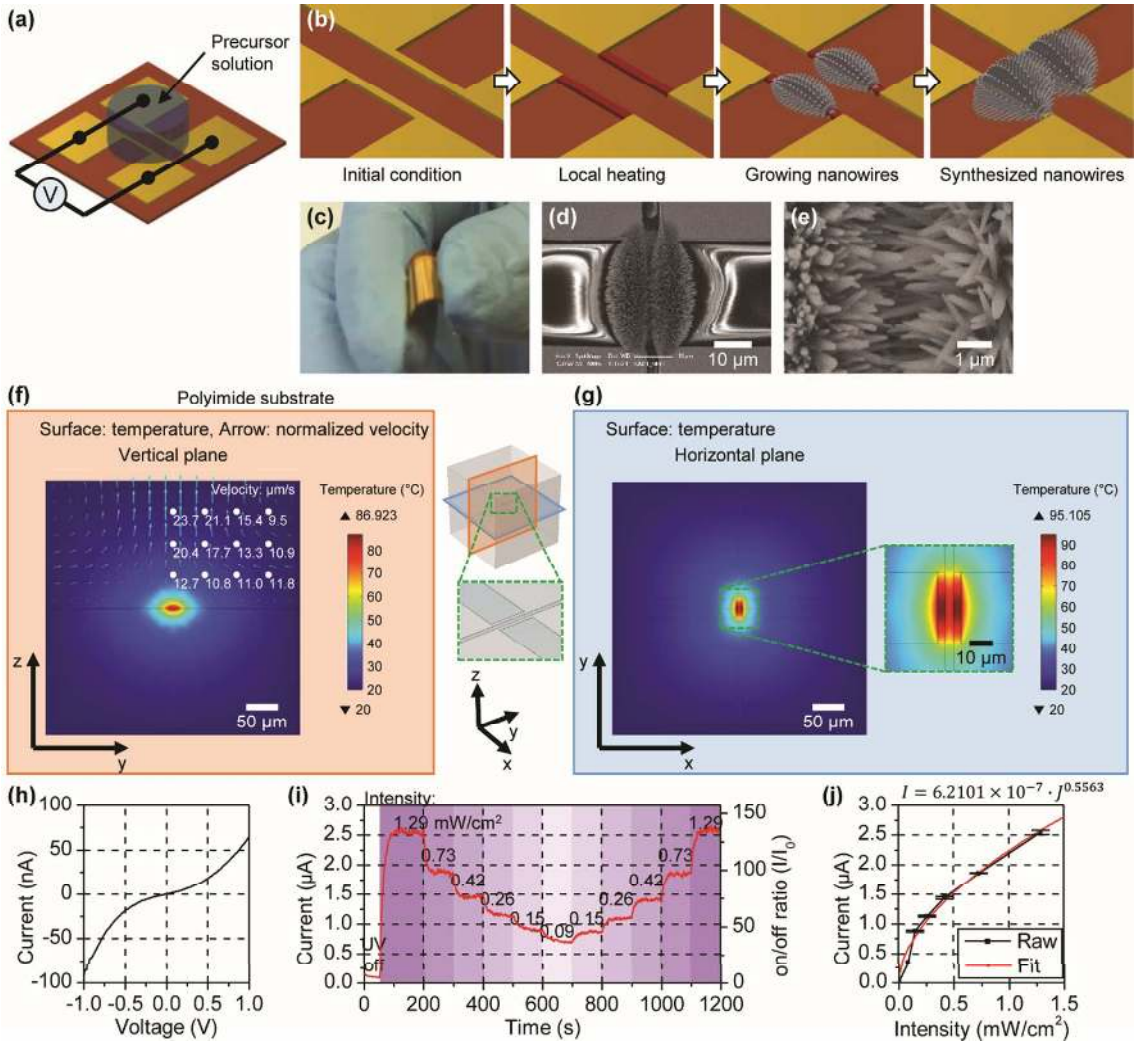

Figure 2. (a) Schematic of experimental setup and (b) process flow for ZnO nanowire synthesis by localized hydrothermal reaction; (c) photo and (d,e) SEM images of locally synthesized ZnO nanowires on a flexible substrate; (f) temperature and flow distribution in the precursor solution and PI substrate during local hydrothermal synthesis process and (g) temperature profile on the surface of the microheater platform on PI substrate; (h) current-voltage (I-V) curve, (i) UV light sensing responses and (j) current on/off ratio vs. illuminance of the fabricated ZnO nanowire sensor.

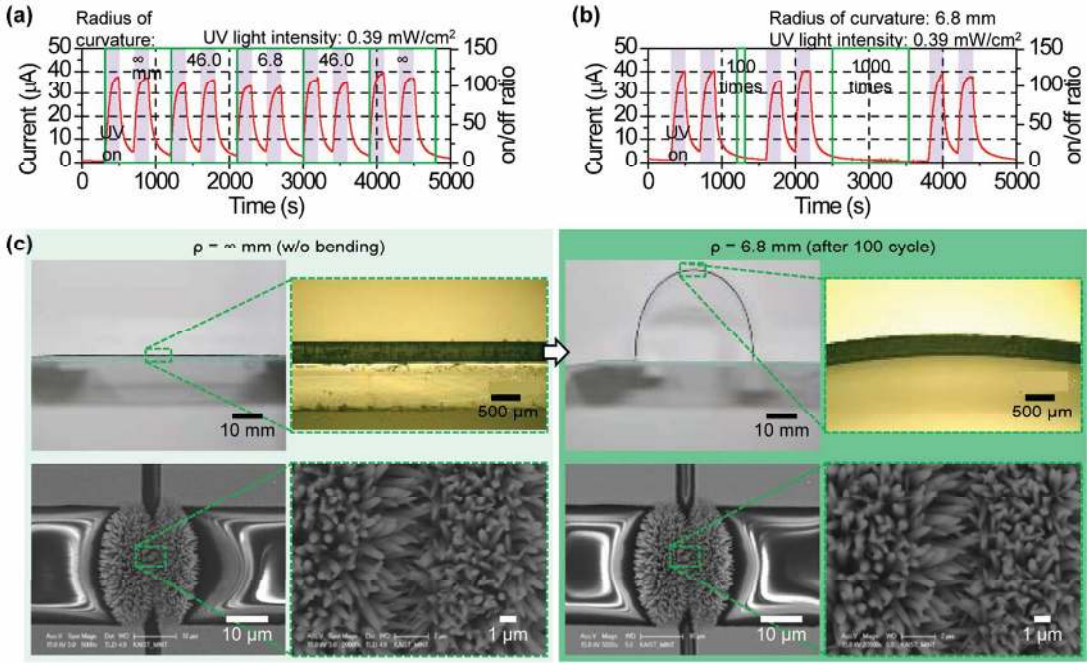

Figure 3. (a) UV light sensing response under various radii of curvature (ρ=∞-6.8 mm) and (b) repeated bending cycles (ρ=6.8 mm); (c) optical and SEM images of ZnO nanowire device under various radii of curvature (ρ=∞, 71.9, 46.0, 26.1, 16.6 and 6.8 mm). There are no notable deformations or cracks in the ZnO nanowires.

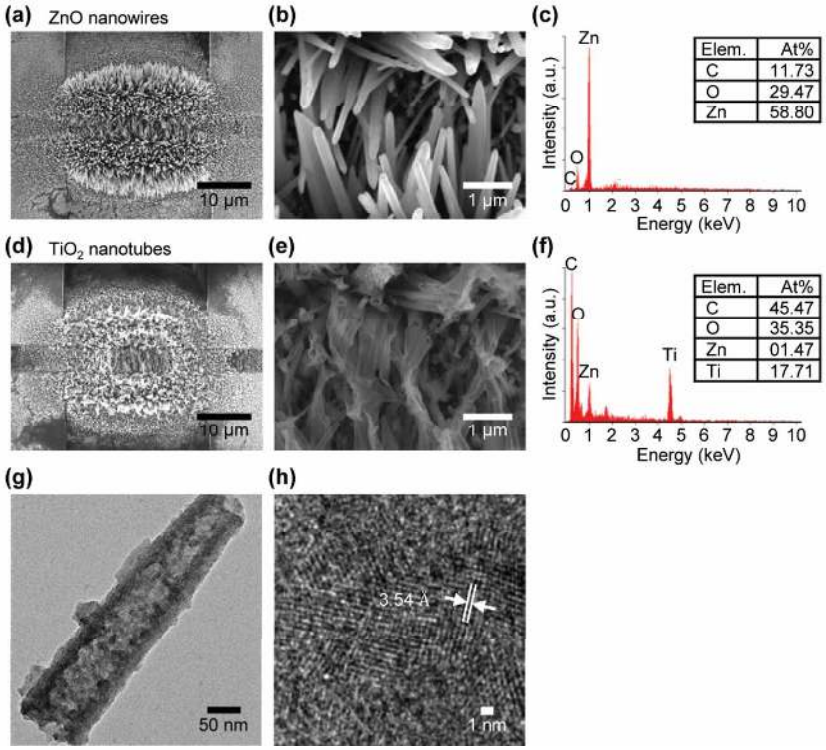

Figure 4. Microstructure and elemental characterization of synthesized ZnO nanowires and TiO_2 nanotubes: (a,b) SEM images and (c) EDS data of ZnO nanowires; (d,e) SEM images, (f) EDS data and (g,h) TEM image of TiO_2 nanotubes.

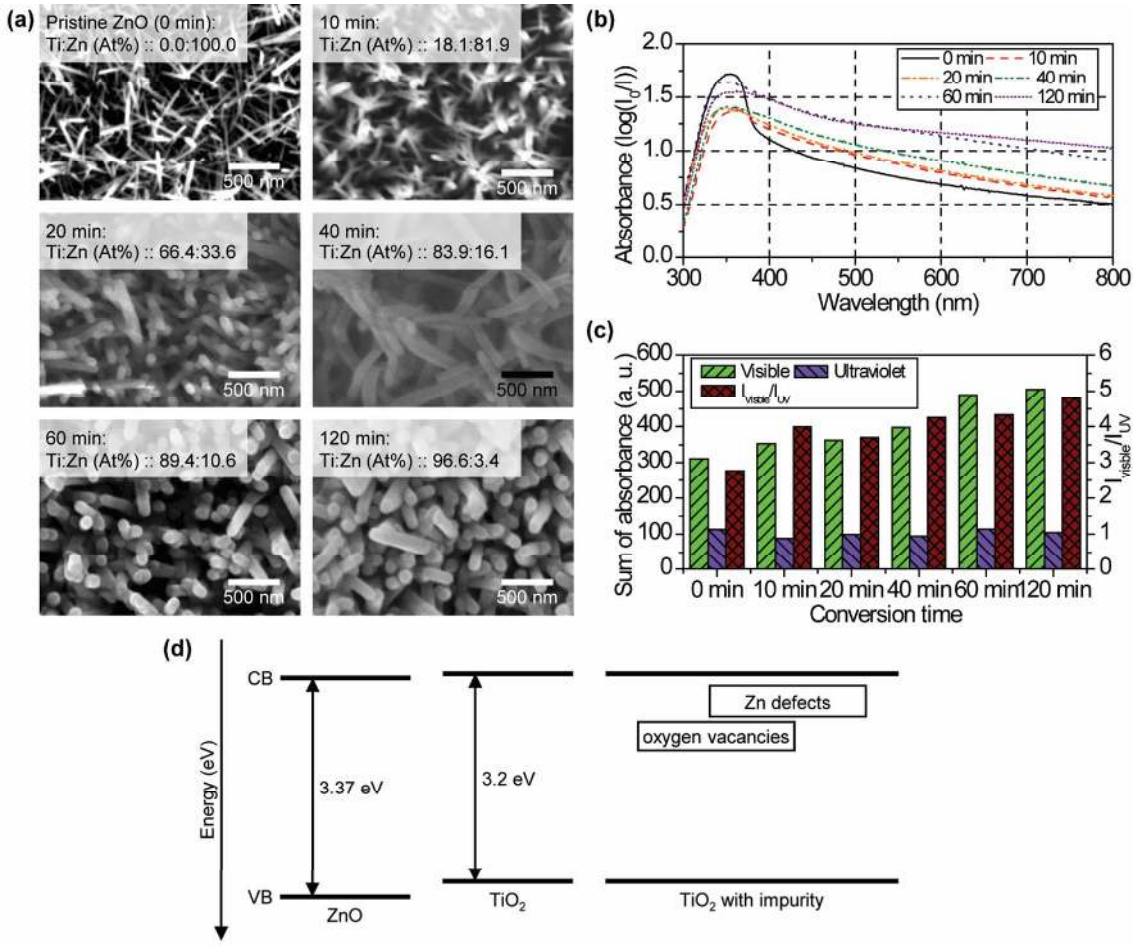

Figure 5. (a) Microstructural change of ZnO-TiO_2 composites after different conversion periods. The diameter of the nanomaterials and atomic ratios of Ti:Zn increase by conversion for longer periods; (b) absorption spectra and (c) absorbance ratio of visible (380-820 nm) to UV (< 380 nm) light region of ZnO-TiO_2 composites. The absorbance of visible light region is increased by increasing the ratio of Ti; (d) energy band diagram of TiO_2 containing oxygen vacancies and Zn defects.

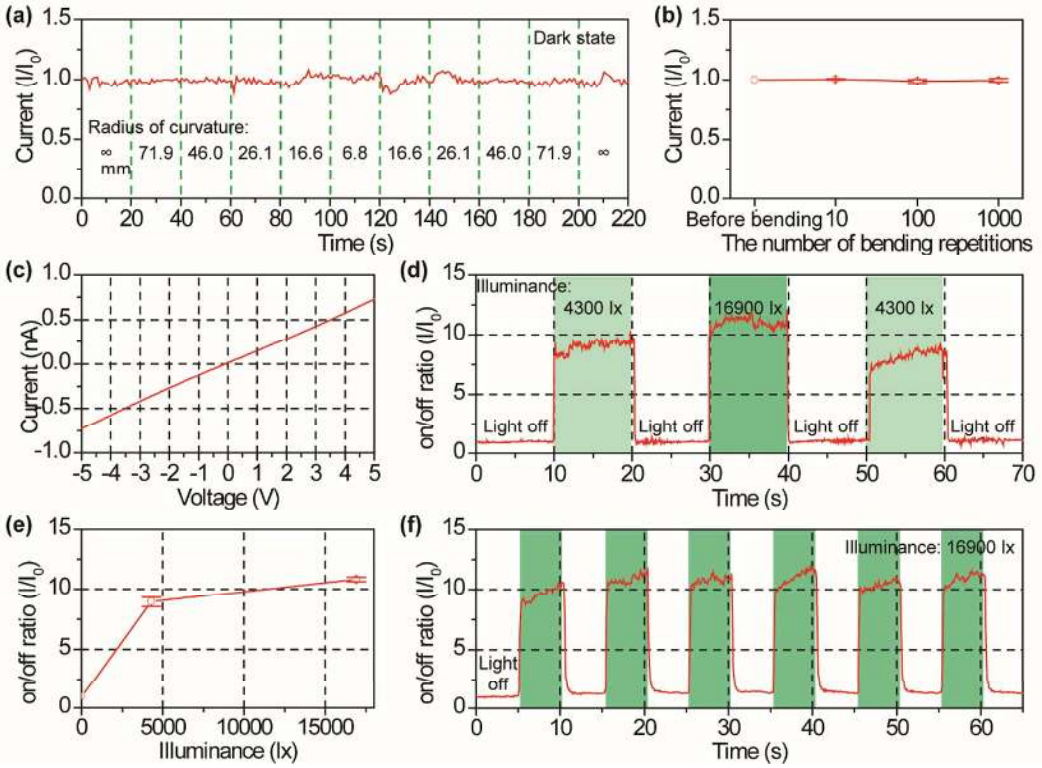

Figure 6. (a) Current through TiO_2 nanotube device under various radii of curvature (ρ=∞, 71.9, 46.0, 26.1, 16.6 and 6.8 mm) and (b) after repeated bending cycles (ρ=6.8 mm); (c) Current-voltage curve of TiO_2 nanotube device; (d) responses of TiO_2 nanotube sensor to various illuminance of ambient light and (e) current on/off ratio vs. illuminance curve; (f) dynamic response under rapid turn-on and turn-off cycles of ambient light.

ASSOCIATED CONTENT

Supporting Information

The following in-depth information is presented in the supporting information: (a) details of microheater device, (b) additional SEM images of ZnO nanowires and TiO_2 nanotubes, (c) numerical simulation of local hydrothermal synthesis method, (d) electrical connection by seed layer, (e) shape of ZnO nanowires under bending condition, (f) ZnO nanowire bending test along the transverse direction to the micro heaters, (g) deformation of nanowires under

bending condition and (h) comparison of light sensing performance. This material is available free of charge via the Internet at http://pubs.acs.org.

AUTHOR INFORMATION

Corresponding Author

*inkyu@kaist.ac.kr

Author Contributions

The manuscript was written through contributions of all authors. All authors have given approval to the final version of the manuscript.

Funding Sources

This research was supported by Nano Material Technology Development Program (2015M3A7B7045518) through the National Research Foundation of Korea (NRF) funded by the Ministry of Science, ICT & Future Planning. This work was also supported by the Center for Integrated Smart Sensors funded by the Ministry of Science, ICT & Future Planning as Global Frontier Project (CISS-2011-0031870)

Notes

The authors declare no competing financial interest.

ACKNOWLEDGMENT

This research was supported by Nano Material Technology Development Program (2015M3A7B7045518) through the National Research Foundation of Korea (NRF) funded by

the Ministry of Science, ICT & Future Planning. This work was also supported by the Center for Integrated Smart Sensors funded by the Ministry of Science, ICT & Future Planning as Global Frontier Project (CISS-2011-0031870)

REFERENCES

1. Xiang, J.; Lu, W.; Hu, Y.; Wu, Y.; Yan, H.; Lieber, C. M. Ge/Si Nanowire Heterostructures as High-Performance Field-Effect Transistors. *Nature*, **2006**, *441*, 489-493.

2. Im, J.-H.; Luo, J.; Franckevicius, M.; Pellet, N.; Gao, P.; Moehl, T.; Zakeeruddin, S. M.; Nazeeruddin, M. K.; Gratzel, M.; Park, N.-G. Nanowire Perovskite Solar Cell. *Nano Lett.* **2015**, *15*, 2120-2126.

3. Xu, S.; Qin, Y.; Xu, C.; Wei, Y.; Yang, R.; Wang, Z. L. Self-Powered Nanowire Devices. *Nat. Nanotechnol.* **2010**, *5*, 366-373.

4. Xia, X.; Tu, J.; Zhang, Y.; Wang, X.; Gu, C.; Zhao, X.-B.; Fan, H. J. High-Quality Metal Oxide Core/Shell Nanowire Arrays on Conductive Substrates for Electrochemical Energy Storage. *ACS Nano*, **2012**, *6*, 5531-5538.

5. Zeng, H.; Xu, X.; Bando, Y.; Gautam, U. K.; Zhai, T.; Fang, X.; Liu, B.; Golberg, D. Template Deformation-Tailored ZnO Nanorod/Nanowire Arrays: Full Growth Control and Optimization of Field-Emission. *Adv. Funct. Mater.* **2009**, 19, 3165-3172.

6. Yang, D.; Kang, K.; Kim, D.; Li, Z.; Park, I. Fabrication of Heterogeneous Nanomaterial Array by Programmable Heating and Chemical Supply within Microfluidic Platform Towards Multiplexed Gas Sensing Application. *Sci. Rep.* **2015**, *5*, 8149.

7. Fu, X.-W.; Liao, Z.-M.; Zhou, Y.-B.; Wu, H.-C.; Bie, Y.-Q.; Xu, J.; Yu, D.-P. Graphene/ZnO Nanowire/Graphene Vertical Structure Based Fast-Response Ultraviolet Photodetector. *Appl. Phys. Lett.* **2012**, *100*, 223114.

8. Yang, D.; Cho. H.; Koo, S.; Vaidyanathan, S. R.; Woo, K.; Yoon, Y.; Choo, H. Simple, Large-Scale Fabrication of Uniform Raman-Enhancing Substrate with Enhancement Saturation. *ACS Appl. Mater. Interfaces* **2017**, *9*, 19092-19101.

9. Athauda, T. J.; Hari, P.; Ozer, R. R. Tuning Physical and Optical Properties of ZnO Nanowire Arrays Grown on Cotton Fibers. *ACS Appl. Mater. Interfaces* **2013**, *5*, 6237-6246.

10. Liu, J.; Wu, W.; Bai, S.; Qin, Y. Synthesis of High Crystallinity ZnO Nanowire Array on Polymer Substrate and Flexible Fiber-Based Sensor. *ACS Appl. Mater. Interfaces* **2011**, *3*, 4197-4200.

11. Prouzet, E.; Ravaine, S.; Sanchez, C.; Backov, R. Bio-Inspired Synthetic Pathways and Beyond: Integrative Chemistry. *New J. Chem.* **2008**, *32*, 1284-1299.

12. Kolmakov, A.; Moskovits, M. Chemical Sensing and Catalysis by One-Dimensional Metal-Oxide Nanostructures. *Annu. Rev. Mater. Res.* **2004**, *34*, 151-180.

13. Yu, H., Li, J., Loomis, R. A., Wang, L.-W., Buhro, W. E. Two-Versus Three-Dimensional Quantum Confinement in Indium Phosphide Wires and Dots, *Nat. Mater.* **2003**, *2*, 517-520.

14. Huang, X.; Zhao, Z.; Chen, Y.; Chiu, C.-Y.; Ruan, L.; Liu, Y.; Li, M.; Duan, X.; Huang, Y. High Density Catalytic Hot Spots in Ultrafine Wavy Nanowires. *Nano Lett.* **2014**, *14*, 3887-3894.

15. Wang, C., Yin, L., Zhang, L., Xiang, D., Gao, R. Metal Oxide Gas Sensors: Sensitivity and Influencing Factors. *Science* **2010**, *10*, 2088-2106.

16. Yang, J.; Hidajat, K.; Kawi, S. Synthesis of Nano-SnO_2/SBA-15 Composite as a Highly Sensitive Semiconductor Oxide Gas Sensor. *Mater. Lett.* **2008**, *62*, 1441-1443.

17. Cui, Y.; Wei, Q.Q.; Park, H.K.; Lieber, C.M. Nanowire Nanosensors for Highly Sensitive and Selective Detection of Biological and Chemical Species. *Science* **2001**, *293*, 1289-1292.

18. Yang, D.; Fuadi, M.K.; Kang, K.; Kim, D.; Li, Z.; Park, I. Multiplexed Gas Sensor Based on Heterogeneous Metal Oxide Nanomaterial Array Enabled by Localized Liquid-Phase Reaction. *ACS Appl. Mater. Interfaces* **2015**, *7*, 10152-10161.

19. Kim, J.; Kwon, S.; Park J.-K.; Park, I. Quantum Dot-Based Immunoassay Enhanced by High-Density Vertical ZnO Nanowire Array. *Biosens. Bioelectron.* **2014**, *55*, 209-215.

20. Tang, Z. K.; Wong, G. K. L.; Yu, P.; Kawasaki, M.; Ohtomo, A.; Koinuma, H.; Segawa, Y. Room-Temperature Ultraviolet Laser Emission from Self-Assembled ZnO Microcrystallite Thin Films. *Appl. Phys. Lett.* **1998**, *72*, 3270-3272.

21. Bai, S.; Wu, W.; Qin, Y.; Cui, N.; Bayerl, D. J.; Wang, X. High-Performance Integrated ZnO Nanowire UV Sensors on Rigid and Flexible Substrates. *Adv. Funct. Mater.* **2011**, *21*, 4464-4469.

22. Alenezi, M. R.; Henley, S. J.; Silva, S. R. P. On-chip Fabrication of High Performance Nanostructured ZnO UV Detectors. *Sci. Rep.* **2014**, *5*, 8516.

23. Wan, Q.; Li, Q.H.; Chen, Y.J.; Wang, T.H.; He, X.L.; Li, J.P.; Lin, C.L. Fabrication and ethanol sensing characteristics of ZnO nanowire gas sensors. *Appl. Phys. Lett.* **2004**, *84*, 3654-3656.

24. Chávez, F.; Pérez-Sánchez, G. F.; Goiz, O.; Zaca-Morán, P.; Peña-Sierra, R.; Morales-Acevedo, A.; Felipec, C.; Soledad-Priego, M. Sensing Performance of Palladium-Functionalized WO_3 Nanowires by a Drop-Casting Method. *Appl. Surf. Sci.* **2013**, *275*, 28-35.

25. Fiorido, T.; Bendahan, M.; Aguir, K.; Bernardini, S.; Martini, C.; Brisset, H.; Fages, F.; Videlot-Ackermannc, C.; Ackermann, J. All Solution Processed Flexible Ammonia Gas and Light Sensors Based on α,ω-Hexyl-Distyrylbithiophene Films. *Sens. Actuators, B* **2010**, *151*, 77-82.

26. Xie, C.; Xiao, L.; Hu, M.; Bai, Z.; Xia, X.; Zeng, D Fabrication and Formaldehyde Gas-Sensing Property of ZnO-MnO_2 Coplanar Gas Sensor Arrays. *Sens. Actuators, B* **2010**, *145*, 457-463.

27. Ul Hasan, K.; Nur, O.; Willander, M. Screen Printed ZnO Ultraviolet Photoconductive Sensor on Pencil Drawn Circuitry Over Paper. *Appl. Phys. Lett.* **2012**, *100*, 211104.

28. Li, B.; Santhanam, S.; Schultz, L.; Jeffries-EL, M.; Iovu, M. C.; Sauvé, G.; Cooper, J.; Zhang, R.; Revelli, J. C.; Kusne, A. G.; *et al.* Inkjet Printed Chemical Sensor Array Based on Polythiophene Conductive Polymers. *Sens. Actuators, B* **2007**, *123*, 651-660.

29. Hsieh, G.-W.; Wang, J.; Ogata, K.; Robertson, J.; Hofmann, S.; Milne, W. I. Stretched Contact Printing of One-Dimensional Nanostructures for Hybrid Inorganic-Organic Field Effect Transistors. *J. Phys. Chem. C* **2012**, *116*, 7118-7125.

30. Yan, Z.; Jureller, J. E.; Sweet, J.; Guffey, M. J.; Pelton, M.; Scherer, N. F. Three-Dimensional Optical Trapping and Manipulation of Single Silver Nanowires. *Nano Lett.* **2012**, *12*, 5155-5161.

31. Reynolds, K.; Komulainen, J.; Kivijakola, J.; Lovera, P.; Iacopino, D.; Pudas, M.; Vähäkangas, J.; Röning, J.; Redmond, G. Probe Based Manipulation and Assembly of Nanowires into Organized Mesostructures. *Nanotechnology* **2008**, *19*, 485301.

32. Heo, K.; Cho, E.; Yang, J.-E.; Kim, M.-H.; Lee, M.; Lee, B. Y.; Kwon, S. G.; Lee, M.-S.; Jo, M.-H.; Choi, H.-J.; Hyeon, T.; Hong, S. Large-Scale Assembly of Silicon Nanowire Network-Based Devices Using Conventional Microfabrication Facilities. *Nano Lett.* **2008**, *8*, 4523-4527.

33. Bellino, M. G.; Calvo, E. J.; Gordillo, G. J. Nanowire Manipulation on Surfaces Through Electrostatic Self-Assembly and Magnetic Interactions. *Phys. Status Solidi RRL* **2009**, *3*, 1-3.

34. Leiterer, C.; Broenstrup, G.; Jahr, N.; Urban, M.; Arnold, C.; Christiansen, S.; Fritzsche, W. Applying Contact to Individual Silicon Nanowires Using a Dielectrophoresis (DEP)-Based Technique. *J. Nanopart. Res.* **2013**, *15*, 1628.

35. Yang, D.; Kim, D.; Ko, S.H.; Pisano, A.P.; Li, Z.; Park I. Focused Energy Field Method for the Localized Synthesis and Direct Integration of 1D Nanomaterials on Microelectronic Devices. *Adv. Mater.* **2015**, *27*, 1207-1215.

36. Pacholski, C.; Kornowski, A.; Weller, H. Self-Assembly of ZnO: From Nanodots to Nanorods. *Angew. Chem. Int. Ed.* **2002**, *41*, 1188-1191.

37. Li, Q.; Kumar, V.; Li, Y.; Zhang, H.; Marks, T. J.; Chang, R. P. H. Fabrication of ZnO Nanorods and Nanotubes in Aqueous Solutions. *Chem. Mater.* **2005**, *17*, 1001-1006.

38. Rule, D. L.; Smith, D. R.; Sparks, L. L. Thermal Conductivity of Polypyromellitimide Film with Alumina Filler Particles from 4.2 to 300 K. *Cryogenics* **1996**, *36*, 283-290.

39. Shanks, H. R.; Maycock, P. D.; Sidles, P. H.; Danielson, G. C. Thermal Conductivity of Silicon from 300 to 1400°K. *Phys. Rev.* **1963**, *130*, 1743-1748.

40. Chien, H.-C.; Yao, D.-J.; Huang, M.-J.; Chang, T.-Y. Thermal Conductivity Measurement and Interface Thermal Resistance Estimation Using SiO_2 Thin Film. *Rev. Sci. Instrum.* **2008**, *79*, 054902.

41. Zumdahl, S. S.; Zumdahl, S. A. *Chemistry*, 7th ed; Houghton Mifflin: Boston, 2007; pp. 790-839.

42. Kim, H.; Moon, J. Y.; Lee, H. S. Growth of ZnO Nanorods on Various Substrates by Electrodeposition. *Electron. Mater. Lett.* **2009**, *5*, 135-138.

43. Jacobi, K.; Zwicker, G.; Gutmann, A. Work Function, Electron Affinity and Band Bending of Zinc Oxide Surfaces. *Surf. Sci.* **1984**, *141*, 109-125.

44. Hansen, W. N.; Johnson, K. B. Work Function Measurements in Gas Ambient. *Surf. Sci.* **1994**, *316*, 373-382.

45. Pierret, R. F. *Semiconductor Device Fundamentals*; Addison-Wesley; Boston, 1996; pp 477-504.

46. Singh, N.; Yan, C.; Lee, P. S.; Comini, E. Sensing Properties of Different Classes of Gases Based on the Nanowire-Electrode Junction Barrier Modulation. *Nanoscale* **2011**, *3*, 1760-1765.

47. Wei, T.-Y.; Yeh, P.-H.; Lu, S.-Y.; Wang, Z. L. Gigantic Enhancement in Sensitivity Using Schottky Contacted Nanowire Nanosensor. *J. Am. Chem. Soc.* **2009**, *131*, 17690-17695.

48. Kind, H.; Yan, H.; Messer, B.; Law, M.; Yang, P. Nanowire Ultraviolet Photodetectors and Optical Switches. *Adv. Mater.* **2002**, *14*, 158-160.

49. Lang, Y.; Gao, H.; Jiang, W.; Xu, L.; Hou, H. Photoresponse and Decay Mechanism of an Individual ZnO Nanowire UV Sensor. *Sens. Actuators, A* **2012**, *174*, 43-46.

50. Yamazoe, N.; Fuchigami, J.; Kishikawa, M.; Seiyama, T. Interactions of Tin Oxide Surface with O_2, H_2O and H_2. *Surf. Sci.* **1979**, *86*, 335-344.

51. Liu, S.; Wang, Z.; Yu, C.; Wu, H. B.; Wang, G.; Dong, Q.; Qiu, J.; Eychmüller, A.; Lou, X. W. A Flexible TiO_2(B)-Based Battery Electrode with Superior Power Rate and Ultralong Cycle Life. *Adv. Mater.* **2013**, *25*, 3462-3467.

52. Suehiro, J.; Nakagawa, N.; Hidaka, S.-I.; Ueda, M.; Imasaka, K.; Higashihata, M.; Okada, T.; Hara, M. Dielectrophoretic Fabrication and Characterization of a ZnO Nanowire-Based UV Photosensor. *Nanotechnology* **2006**, *17*, 2567-2573

53. A. Rose, *Concepts in Photoconductivity and Allied Problems*; Interscience Publishers; New York, 1963; pp 33-43.

54. Beer, F.; Johnston Jr., E. R.; DeWolf, J.; Mazurek, D. *Mechanics of Materials*, 6th ed; McGraw-Hill; New York, 2011; pp 221-233.

55. Tang, H.; Berger, H.; Schmid, P. E.; Lévy, F.; Burri, G. Photoluminescence in TiO_2 Anatase Single Crystals. *Solid State Commun.* **1993**, *87*, 847-850.

56. Deki, S.; Aoi, Y.; Hiroi, O.; Kajinami, A. Titanium (IV) Oxide Thin Films Prepared from Aqueous Solution. *Chem. Lett.* **1996**, *1996*, 433-434.

57. Xu, C.; Shin, P. H.; Cao, L.; Wu, J.; Gao, D. Ordered TiO_2 Nanotube Arrays on Transparent Conductive Oxide for Dye-Sensitized Solar Cells. *Chem. Mater.* **2010**, *22*, 143-148.

58. Lee, J.-H.; Leu, I.-C.; Hsu, M.-C.; Chung, Y.-W.; Hon, M.-H. Fabrication of Aligned TiO_2 One-Dimensional Nanostructured Arrays Using a One-Step Templating Solution Approach. *J. Phys. Chem. B* **2005**, *109*, 13056-13059.

59. Wisitsoraat, A.; Tuantranont, A.; Comini, E.; Sberveglieri, G.; Wlodarski, W. Characterization of n-Type and p-Type Semiconductor Gas Sensors Based on NiO_x Doped TiO_2 Thin Films. *Thin Solid Films* **2009**, *517*, 2775-2780.

60. He, J.; Behera, R. K.; Finnis, M. W.; Li, X.; Dickey, E. C.; Phillpot, S. R.; Sinnott, S. B. Prediction of High-Temperature Point Defect Formation in TiO_2 from Combined Ab initio and Thermodynamic Calculations. *Acta Mater.* **2007**, *55*, 4325-4337.

61. Nakamura, I.; Negishi, N.; Kutsuna, S.; Ihara, T.; Sugihara, S.; Takeuchi, K. Role of Oxygen Vacancy in the Plasma-Treated TiO_2 Photocatalyst with Visible Light Activity for NO Removal. *J. Mol. Catal. A: Chem.* **2000**, *161*, 205-212.

62. Yang, L.; Zhang, Y.; Ruan, W.; Zhao, B.; Xu, W.; Lombardi, J. R. Improved Surface-Enhanced Raman Scattering Properties of TiO_2 Nanoparticles by Zn Dopant. *J. Raman Spectrosc.* **2010**, *41*, 721-726.

63. Cao, C.; Hu, C.; Wang, X.; Wang, S.; Tian, Y.; Zhang, H. UV Sensor Based on TiO_2 Nanorod Arrays on FTO Thin Film. *Sens. Actuators, B* **2011**, *156*, 114-119.

64. Xiao, P.; Liu, D.; Garcia, B. B.; Sepehri, S.; Zhang, Y.; Cao, G. Electrochemical and Photoelectrical Properties of Titania Nanotube Arrays Annealed in Different Gases. *Sens. Actuators, B* **2008**, *134*, 367-372.

65. Smith, G. X. R.; Crook, R.; Wadhawan, J. D. Measuring the Work Function of TiO_2 Nanotubes Using Illuminated Electrostatic Force Microscopy. *J. Phys.: Conf. Ser.* **2013**, *471*, 012045.

66. Paulose, M.; Varghese, O. K.; Mor, G. K.; Grimes, C. A.; Ong, K. G. Unprecedented Ultra-High Hydrogen Gas Sensitivity in Undoped Titania Nanotubes. *Nanotechnology* **2006**, *17*, 398-402.

67. Mamat, M. H.; Ishak, N. I.; Khusaimi, Z.; Zahidi, M. M.; Abdullah, M. H.; Muhamad, S.; Sin, N. D. M.; Mahmood, M. R. Thickness-Dependent Characteristics of Aluminium-Doped Zinc Oxide Nanorod-Array-Based, Ultraviolet Photoconductive Sensors. *Jpn. J. Appl. Phys.* **2012**, *51*, 06FF03.

TOC Figure

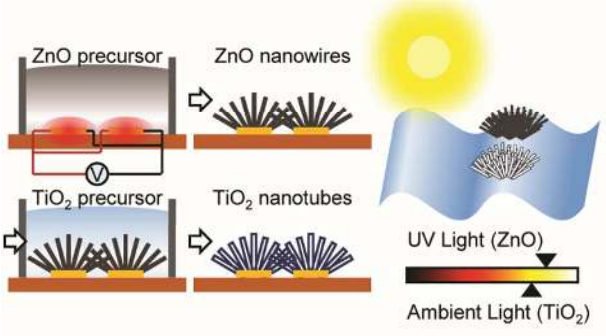
ZnO precursor
ZnO nanowires
TiO2 precursor
TiO2 nanotubes
UV Light (ZnO)
Ambient Light (TiO2)

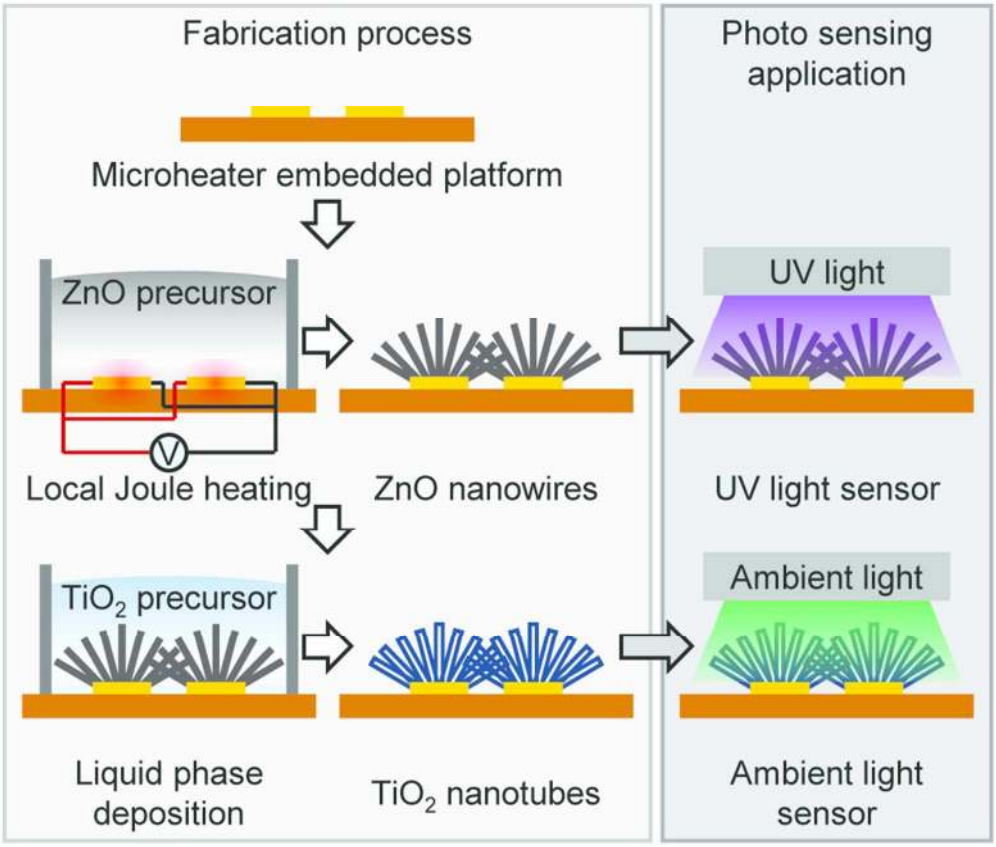

Figure 1. Schematic of process flow for the ZnO nanowire and TiO_2 nanotube synthesis. ZnO nanowires are synthesized by local hydrothermal reaction along microheaters and pre-synthesized ZnO nanowires are converted to TiO_2 nanotubes by liquid phase deposition.

85x72mm (300 x 300 DPI)

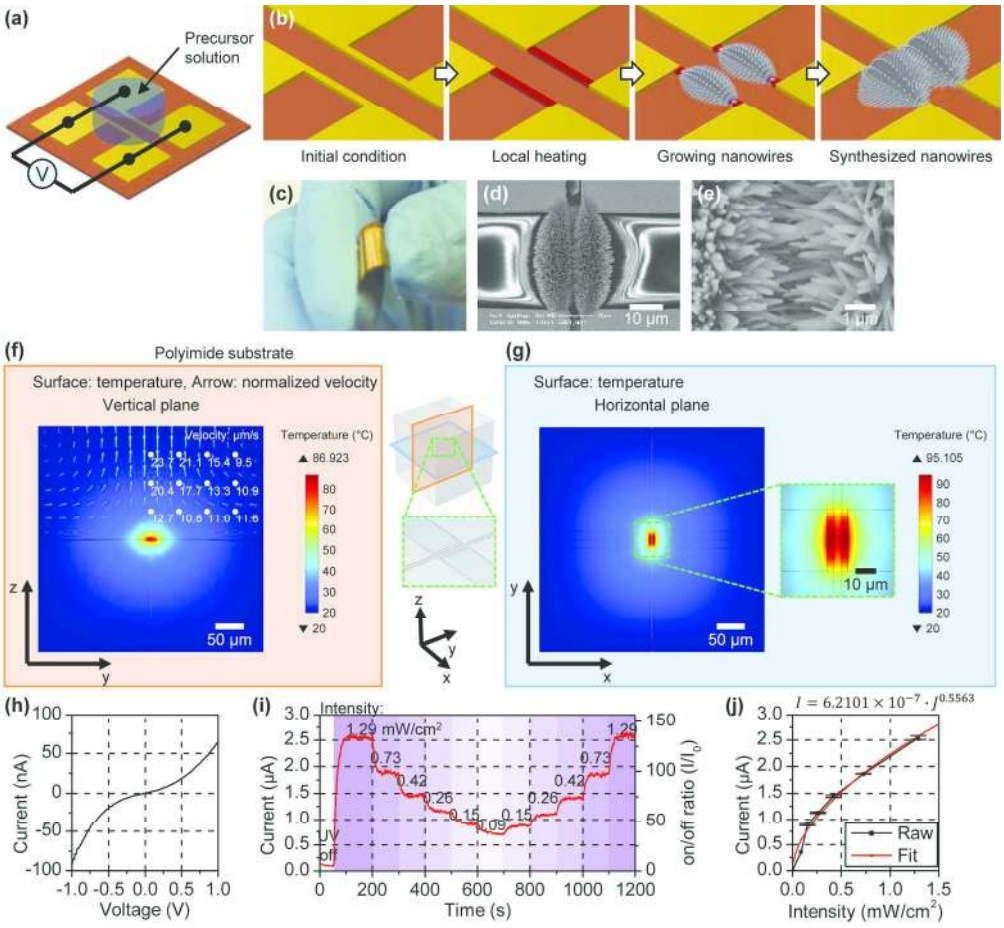

Figure 2. (a) Schematic of experimental setup and (b) process flow for ZnO nanowire synthesis by localized hydrothermal reaction; (c) photo and (d,e) SEM images of locally synthesized ZnO nanowires on a flexible substrate; (f) temperature and flow distribution in the precursor solution and PI substrate during local hydrothermal synthesis process and (g) temperature profile on the surface of the microheater platform on PI substrate; (h) current-voltage (I-V) curve, (i) UV light sensing responses and (j) current on/off ratio vs. illuminance of the fabricated ZnO nanowire sensor.

178x163mm (300 x 300 DPI)

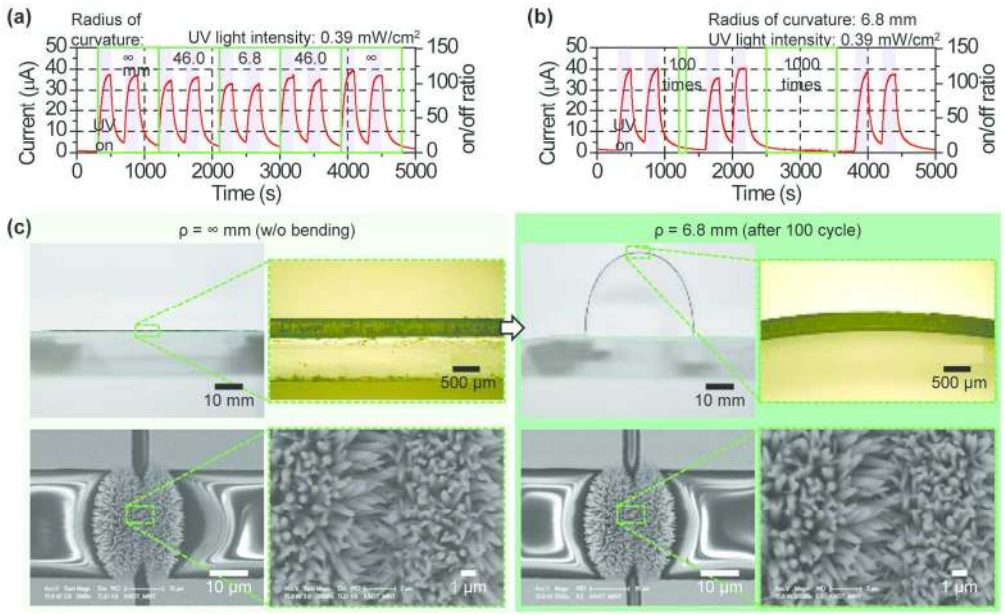

Figure 3. (a) UV light sensing response under various radii of curvature (ρ=∞-6.8 mm) and (b) repeated bending cycles (ρ=6.8 mm); (c) optical and SEM images of ZnO nanowire device under various radii of curvature (ρ=∞, 71.9, 46.0, 26.1, 16.6 and 6.8 mm). There are no notable deformations or cracks in the ZnO nanowires.

171x104mm (300 x 300 DPI)

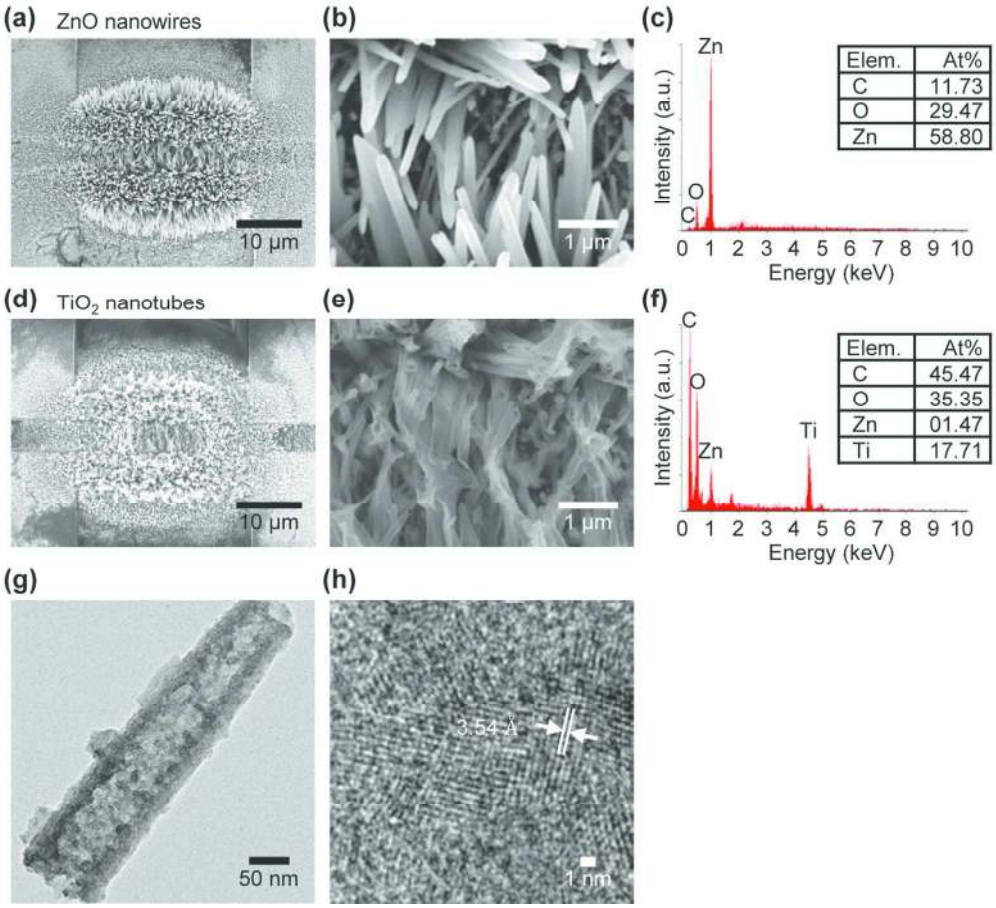

Figure 4. Microstructure and elemental characterization of synthesized ZnO nanowires and TiO_2 nanotubes: (a,b) SEM images and (c) EDS data of ZnO nanowires; (d,e) SEM images, (f) EDS data and (g,h) TEM image of TiO_2 nanotubes.

131x119mm (300 x 300 DPI)

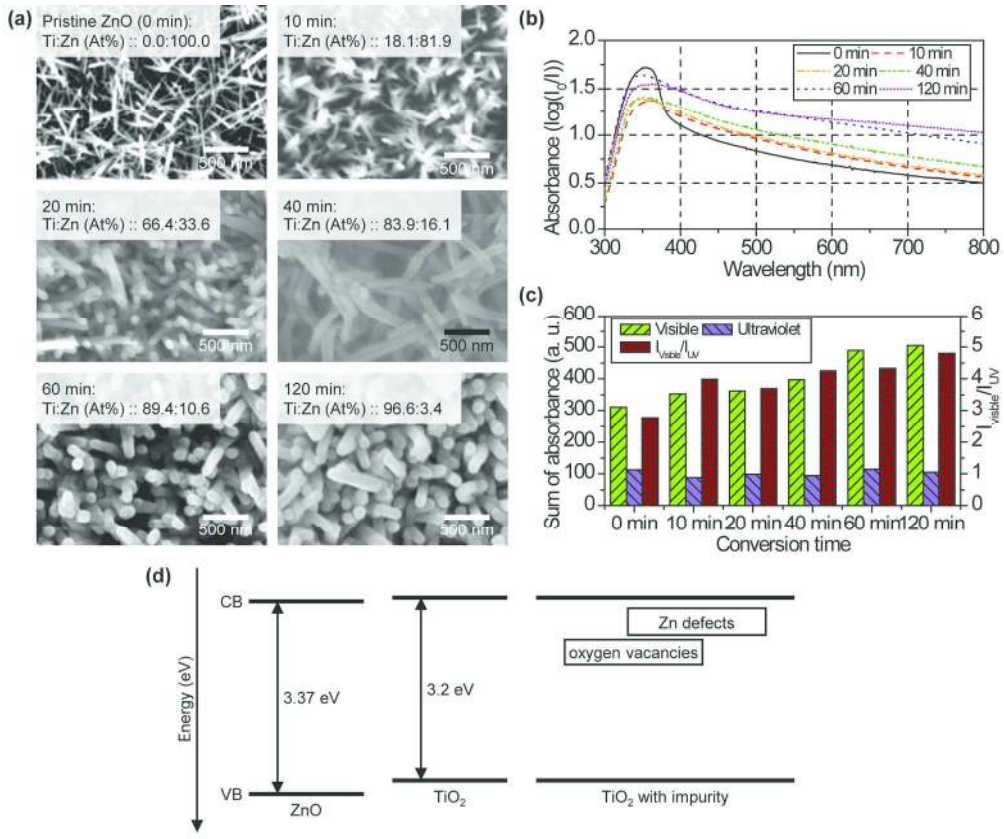

Figure 5. (a) Microstructural change of ZnO-TiO_2 composites after different conversion periods. The diameter of the nanomaterials and atomic ratios of Ti:Zn increase by conversion for longer periods; (b) absorption spectra and (c) absorbance ratio of visible (380-820 nm) to UV (< 380 nm) light region of ZnO-TiO_2 composites. The absorbance of visible light region is increased by increasing the ratio of Ti; (d) energy band diagram of TiO_2 containing oxygen vacancies and Zn defects.

174x145mm (300 x 300 DPI)

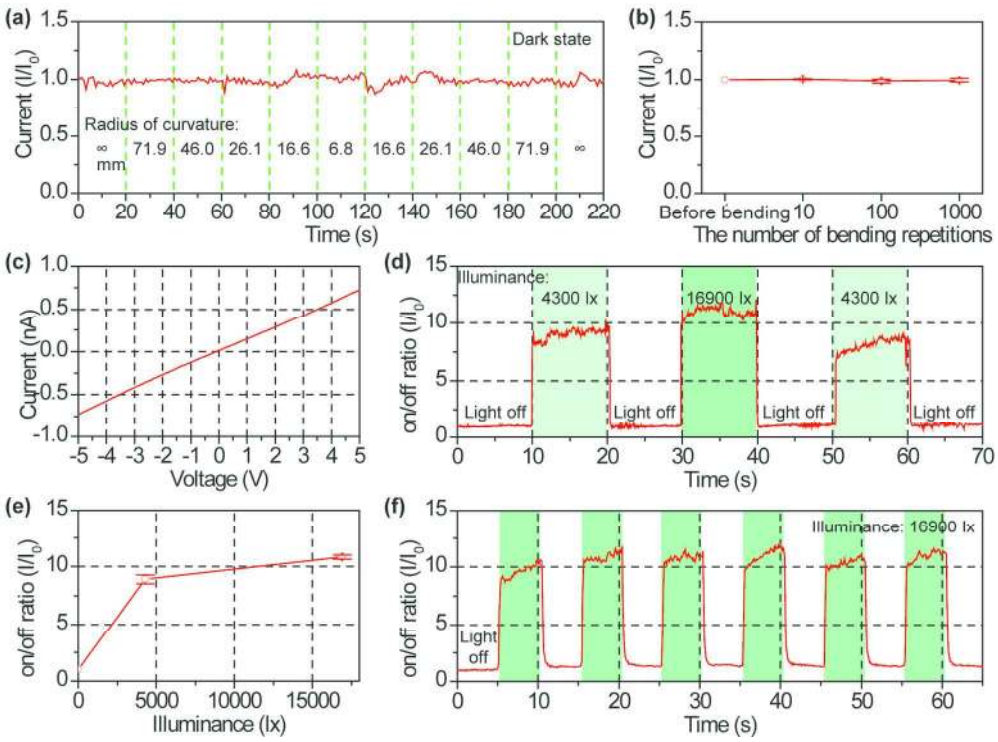

Figure 6. (a) Current through TiO_2 nanotube device under various radii of curvature (ρ=∞, 71.9, 46.0, 26.1, 16.6 and 6.8 mm) and (b) after repeated bending cycles (ρ=6.8 mm); (c) Current-voltage curve of TiO_2 nanotube device; (d) responses of TiO_2 nanotube sensor to various illuminance of ambient light and (e) current on/off ratio vs. illuminance curve; (f) dynamic response under rapid turn-on and turn-off cycles of ambient light.

163x120mm (300 x 300 DPI)